Proc. Natl. Acad. Sci. USA
Vol. 95, pp. 9262–9267, August 1998
Biophysics

Single-particle selection and alignment with heavy atom cluster-antibody conjugates

(Nanogold/single-chain Fv antibody fragments/cryoelectron microscopy/image processing/three-dimensional reconstruction)

GRANT J. JENSEN AND ROGER D. KORNBERG*

Department of Structural Biology, Stanford University School of Medicine, Stanford, CA 94305

Contributed by Roger D. Kornberg, May 26, 1998

ABSTRACT **A method is proposed for selecting and aligning images of single biological particles to obtain high-resolution structural information by cryoelectron microscopy. The particles will be labeled with multiple heavy atom clusters to permit the precise determination of particle locations and relative orientations even when imaged close to focus with a low electron dose, conditions optimal for recording high-resolution detail. Heavy atom clusters should also allow selection of images free from many kinds of defects, including specimen movement and particle inhomogeneity. Heavy atom clusters may be introduced in a general way by the construction of "adaptor" molecules based on single-chain Fv antibody fragments, consisting of a constant framework region engineered for optimal cluster binding and a variable antigen binding region selected for a specific target. The success of the method depends on the mobility of the heavy atom cluster on the particle, on the precision to which clusters can be located in an image, and on the sufficiency of cluster projections alone to orient and select particles for averaging. The necessary computational algorithms were developed and implemented in simulations that address the feasibility of the method.**

Electron microscopy of biological specimens is limited in resolution by beam-induced specimen damage because single organic molecules are destroyed by electron irradiation sufficient to reveal structural details. In addition to damaging the specimen, electrons, even at low doses, impair the quality of electron imaging by causing localized heating, specimen movement, and specimen charging. These difficulties can be overcome by image averaging and special data collection techniques (1–3). The possibility of structure determination to atomic resolution has been indicated (4) and in some cases attained (2, 5, 6).

Image averaging to improve the signal-to-noise ratio of low-dose electron micrographs has been accomplished in the past by diffraction from ordered arrays of molecules or by computational methods of aligning the images of single particles. Development of the diffraction approach exploited naturally occurring ordered arrays, such as virus particles, muscle fibers, and two-dimensional (2-D) crystals of membrane proteins (7, 8). A general method of forming 2-D crystals was devised to bring a wide range of proteins within reach of the approach (9). The necessity of forming a crystalline specimen nonetheless remains an impediment. It prevents the study of a great many biological objects, including partially irregular or inhomogeneous molecules and molecular complexes. The very large multiprotein complexes of most biological interest are especially prone to these limitations.

Escape from the requirement for crystals by computational alignment of single particles relies on the detection of image details to determine the relative orientations of the particles and permit image averaging (10). The very paucity of detail in a low-dose electron micrograph that necessitates averaging unavoidably limits the precision of alignment for the purpose of averaging. Alignment is made possible by recording images at high defocus values, which results in a loss of contrast at high resolution.

An approach is proposed here for extending the range and resolution of structure determination by electron microscopy through derivatization with heavy atom clusters. This approach is applicable to single molecules and avoids reliance on molecular details for averaging, allowing alignment of images recorded very close to focus. It overcomes technical limitations, including detection of drift, particle inhomogeneity, and magnification variation. It may also allow manipulation of particle orientations and analysis of orders of magnitude more particles because of greater computational speed, possibly enabling the structure determination of even comparatively small proteins to quite high resolution.

PROPOSED METHOD

The particle of interest will be labeled with multiple heavy atom clusters large enough for precise localization in low-dose electron micrographs. Labeling at four sites should suffice for determination of the molecular orientation, enabling image averaging and three-dimensional (3-D) reconstruction. Although labeling could be direct, a more general method would employ an adaptor, such as an antibody fragment, derivatized with a heavy atom cluster. The framework region of an antibody may be modified to immobilize a suitable heavy atom cluster, and the variable region of this modified antibody can then be selected for a wide range of specificities.

FEASIBILITY

There are three requirements for success of the proposed method. First, heavy atom clusters must be identified that are large and dense enough to be imaged at high resolution under conditions optimal for recording atomic detail from vitrified biological specimens. Second, multiple heavy atom clusters must be attached rigidly to biological specimens in a generally applicable way. Third, the projection of some number of clusters must suffice to select and orient particles for averaging.

Heavy Atom Clusters for Electron Microscopy. Heavy atom clusters that can be imaged clearly under appropriate conditions have already been described. Nanogold particles, which contain 67 gold atoms in an approximately spherical volume,

The publication costs of this article were defrayed in part by page charge payment. This article must therefore be hereby marked "*advertisement*" in accordance with 18 U.S.C. §1734 solely to indicate this fact.

© 1998 by The National Academy of Sciences 0027-8424/98/959262-6$2.00/0
PNAS is available online at www.pnas.org.

Abbreviations: 3-D, three-dimensional; scFv, single-chain Fv antibody fragment.

*To whom reprint requests should be addressed. e-mail: kornberg@stanford.edu.

14 Å in diameter (11), are readily visible under low-dose conditions, close to focus, frozen in thin layers of vitreous ice (12–18). In particular, when imaged at 0.5-μm underfocus, Nanogold particles have a diameter near the expected size (16). The circular symmetry of the particles should then allow the center to be located to near atomic resolution.

The ideal heavy atom cluster would be the smallest clearly visible particle, and several candidates exist, including Au_{39} (19), Au/Ag alloys of 25, 37, and 38 heavy atoms (20), W_{30} (21), Ni_{34} (22), Ni_{38} (23), and Pd_{38} (24). The minimal visible cluster has not been determined, but Undecagold, which contains 11 gold atoms in an approximately spherical volume 8 Å in diameter, is not seen in individual images at low dose, and it can be located only by averaging many particles, for example over a two-dimensional array (25).

Heavy Atom Cluster-Antibody Conjugates. The feasibility of immobilizing heavy atom clusters on biological macromolecules has been demonstrated by x-ray crystallographic studies employing clusters for phase determination. Crystals are generally soaked in solutions of various cluster compounds, and binding of the clusters is assessed by diffraction analysis. Such an empirical approach is not well suited to our requirements. We can, however, exploit an advantage of single particles over crystals that the surface of the particle is exposed, allowing the introduction of additional molecules as "adaptors." In particular, we propose here the use of an antibody fragment to rigidly bind both the heavy atom cluster and the particle to be imaged. As intact antibodies are bivalent, and Fab fragments have a flexible elbow region (26), Fv fragments are the best choice. Fv fragments are also preferable because they are small (25 kDa), making them less likely to obstruct one another. Furthermore, Fvs can be engineered as single polypeptide chains (scFvs), readily manipulated genetically, and easily expressed in bacteria. Fvs comprise a variable antigen-binding surface supported by a constant framework region. We anticipate engineering heavy atom cluster binding sites within the framework region of an scFv, for instance by introducing surface cysteine residues. Techniques such as random mutagenesis of the antigen-binding region and phage display can be used to select desired antigen binding specificities. Although immobilization of the heavy atom cluster is important, single-particle alignment adequate for atomic resolution structure determination does not require that the cluster be perfectly fixed. Rather, some flexibility may be tolerated, as shown by the computer simulations of the alignment process described below.

Selection and Alignment. Selection and alignment may be accomplished in two stages: first, determination of the relative 3-D coordinates of the clusters bound to the particle; and second, determination of the relative orientations of particles from cluster projections. One procedure for the first stage is to record a pair of images, tilted with respect to one another, and calculate 3-D coordinates of the clusters on the basis of the known direction and magnitude of tilt. The result may be refined by averaging over many particles. Given the coordinates of the clusters with respect to one another on the particle, as well as the projection pattern of a randomly rotated particle, the second stage of alignment is accomplished by finding the set of rotation angles that gives rise to the projection. We refer to such a set of rotation angles as a "match." Finding rotation angles from a single untilted image is made possible by transformation of particles to a center of mass system in which equations relating the rotation angles, the original cluster configuration, and the projection pattern can be solved for the rotation angles (*Appendix*). Because the set of possible projection patterns from a given cluster configuration is finite, selection can be accomplished simultaneously with alignment by eliminating particles whose projection patterns do not match any rotation of the original cluster coordinates, and must therefore be derived from deformed cluster configurations.

The number of clusters needed to select and align particles on the basis of projection patterns can be estimated *a priori*. The projection pattern of three clusters will always leave an ambiguity in orientation because they are coplanar, and the sign of the tilt angle relating the cluster plane and the projection plane is indeterminate. A second, tilted image of the particle might be used to resolve this ambiguity. Alternatively, four or more noncoplanar, nonsymmetrically distributed clusters should suffice for orientation determination. In the case of four clusters per particle, eight independent equations can be obtained for the three rotation angles relating cluster projections to the cluster coordinates. These equations can be solved for all 24 (4 factorial) possible assignments of clusters in the projection to clusters on the particle, and all possible matches can be checked for ambiguity.

SIMULATIONS

Four simulations were performed to demonstrate the two stages involved in selection and alignment and to explore how flexibility in cluster positions and error in location of these positions would compromise the results. The first simulation mimicked the first stage of alignment by determining the relative 3-D coordinates of clusters bound to the particle from two simulated, tilted images of a particle field. The second, third, and fourth simulations were variations of the second stage of alignment, and they explored the choice of alignment parameters, the median angular alignment error, and the utility of cluster labeling for selection of homogeneous (undeformed) particles, respectively.

Determination of Cluster Coordinates. The first step in the proposed method would be to label a particle of interest with at least four heavy atom clusters and then determine their relative 3-D positions. We simulated determination of the relative cluster positions from two images of a field of particles, one tilted 45° with respect to the other. Flexibility in cluster positions was represented by a "cluster-noise" parameter, which defines the maximum, random, radial displacement of a cluster from its assigned location. In addition, an "EM-noise" parameter was introduced to model the maximum, random, radial error in locating the center of a heavy atom cluster in a micrograph. The algorithm was to generate a model particle with random cluster locations on the surface, rotate it in space by three random rotation angles, displace the cluster positions randomly within a sphere of radius "cluster-noise," record projection coordinates including a random "EM-noise" displacement, rotate the particle by an additional 45° about a known tilt axis, record a second set of projection coordinates including another random "EM-noise" displacement, and finally calculate x, y, and z coordinates for each cluster based on these two sets of projection coordinates. We assumed in the simulation that corresponding particles and clusters in the tilted images were previously identified as well as the direction and magnitude of tilt, noting that algorithms for these tasks are routine and well established (10, 27, 28). The accuracy of the procedure then depends mostly on the uniformity of cluster positions with respect to the particle (cluster-noise), on the precision to which clusters can be located in the micrograph (EM-noise), and on the number of particles averaged.

The resulting cluster coordinates for each succeeding particle were averaged into a running model, and the average radial coordinate error for any particular cluster after n particles was averaged with 500 different iterations of this algorithm, using different, randomly derived, cluster configurations (Fig. 1). The maximum and minimum radial cluster coordinates (100 Å and 60 Å, respectively) were appropriate for a 500-kDa protein of expected radius 52 Å, with an additional radial extension of 28 Å because of the scFv. Randomness was constrained by a minimum cluster–cluster distance of 38 Å, the diameter of an scFv. This simulation

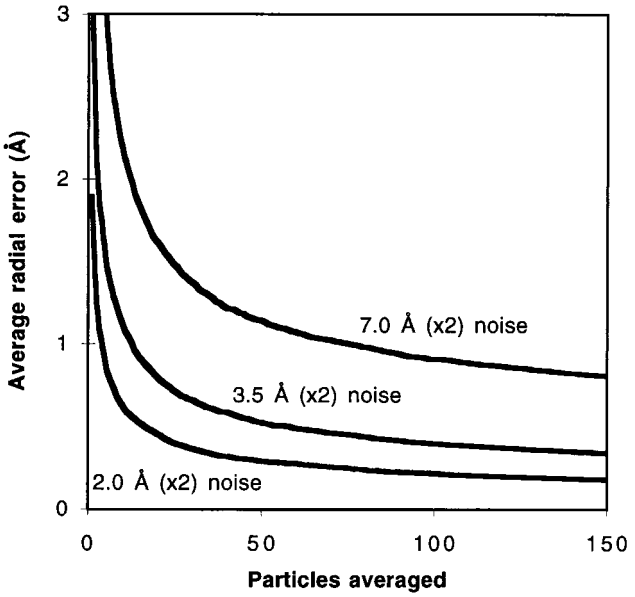

FIG. 1. Accuracy of original cluster coordinate determination. The average radial error in a cluster position is shown for differing levels of noise after results from n particles are averaged. The three curves represent simulations in which projected coordinates are randomly displaced by the given amount of noise twice: once to model the cluster's movement with respect to the particle, and again to model error in locating the cluster's center in the micrograph. Each curve is the average error after n particles for 500 different iterations of the procedure, each beginning with a unique, randomly generated cluster configuration.

showed, for example, that if the center of the heavy atom cluster is free to move on the surface of the scFv within a sphere of radius 7 Å (the radius of Nanogold), and if we can determine the position of the center of the heavy atom cluster on the micrograph to within 7 Å, it would take about 75 particle pairs to determine the original 3-D coordinates of the clusters to within 1 Å, given perfect knowledge of the direction and magnitude of tilt. Of course, a tilt series including multiple tilts could also be taken to reduce the number of particles needed.

Alignment Parameters. Once the relative positions of clusters on a particle are known, these can be used to select and align the projections of randomly rotated particles. For the second, third, and fourth simulations a program was written to demonstrate and explore this process. The algorithm generated a random cluster configuration as described, rotated it by random angles, recorded the cluster projection pattern with random displacements to simulate noise, and searched for the rotation angle sets that gave rise to the observed projection pattern. When no noise was added, virtually all particles were uniquely matched to exact rotation angles, and particle deformities were easily detected (Table 1, row 1).

In the presence of noise, however, a particular particle rotation can result in a range of observed projection patterns, and criteria were established to decide whether a set of rotation angles and its corresponding projection pattern (as predicted from the cluster coordinates) "matched" the observed, noisy pattern. First, the "spatial match error" was defined as the maximum radial coordinate error seen between a pair of corresponding clusters in the two patterns. The first alignment parameter was then called the "spatial match threshold" and was defined as the largest spatial match error that could exist between two projection patterns for them to be considered as arising from the same set of rotation angles. Thus for a projection pattern to be matched to a set of rotation angles, each cluster on the particle was required to have a predicted position within the spatial match threshold of a corresponding observed cluster position.

Further ambiguities arose in the assignment of matches because projection patterns varied continuously with rotation angle and because projection patterns resulting from widely separated sets of rotation angles were in some cases nearly identical. For any particular noisy projection pattern, there were no sets of rotation angles, one set, or more than one set found that fell within the spatial match threshold. In cases where there were more than one, either the sets were close together in angular space, representing different approximations to the correct rotation angles with varying accuracy, or the sets were widely separated and demonstrated true ambiguity. A second alignment parameter, the "angular ambiguity threshold," was therefore defined as the maximum angular difference in any rotation angle between two sets of rotation angles that was allowed for the two sets to be considered as different approximations of a single unique match. If any difference in any rotation angle between two angular sets that matched a projection pattern was greater than the angular ambiguity threshold, the pattern was regarded as ambiguous, and the particle could not be uniquely aligned by this method. Reasonable values for the angular ambiguity threshold for a particular level of noise were chosen as a minimum of 2° plus twice the expected angular alignment error, which is the inverse sine of the average noise (half the maximum) divided by the average radial coordinate (80 Å here).

With these alignment parameters defined, there were four possible outcomes for each particle projection in the simulations. The first is that the projection was uniquely matched to a set of rotation angles close to the actual angles used to rotate the particle ("correctly matched"). The second is that the projection was ambiguous, meaning that more than one set of matching angles, further apart than the angular ambiguity threshold, was found ("ambiguous"). The third is that no matches were found, which occurred when the introduction of

Table 1. Statistics for the simulated alignment of 500 randomly rotated particles of each of 500 randomly generated configurations with four clusters per particle

Noise, Å	% correctly matched	% mistakenly matched	Median angular error for correct matches, °	% deformed particles excluded (45° domain shift)
0	100.0	0.00	0.00	99.9
1	96.2	0.04	0.25	99.2
2	91.8	0.26	0.50	98.3
3	85.6	0.73	0.75	97.3
4	81.5	1.10	0.99	96.0
5	75.6	1.91	1.26	94.6
6	70.6	2.47	1.49	93.1
7	64.2	3.29	1.73	91.4

In cases where the absolute value of β was over 81° (see *Appendix* for the definition of α, β, and γ), α and γ were either added or subtracted before calculating an error, because as β approaches 90° or −90° only the sum or difference of these angles is geometrically relevant, respectively.

noise perturbed the projection pattern outside the spatial match threshold, and these particles were erroneously discarded as deformed ("unmatched"). The fourth possibility was that the correct set of angles was not found, but an erroneous set of angles did happen to match ("mistakenly matched"). This last category of projections was identified because the unique match angles obtained were much different from those actually used to produce the patterns. Such mistakenly matched particles would add a small amount of random noise to a final 3-D reconstruction, as their angles are completely unrelated to the correct angles.

The results of earlier simulations showed that for typical cluster configurations, less than 20% of random projections were ambiguous for moderate spatial match thresholds. Because at high resolution, continuous missing cones of reciprocal space containing as much as 14% of the data have no serious effect on a 3-D reconstruction (29), and because the ambiguous projections were widely distributed in angular space rather than concentrated in a continuous missing cone (data not shown), the existence of these ambiguous projections should not significantly limit the outcome of our procedure. There was, however, a population of random configurations that produced much higher percentages (as many as 100%) of ambiguous projections. These configurations happened to be nearly coplanar or to exhibit symmetry relationships among the clusters, the worst case being full tetrahedral symmetry. In practice, many scFv-heavy atom cluster conjugates will be identified for labeling the particle of interest, and if a particular set of four produces a high percentage of ambiguous projections, other conjugates could be used. With this possibility in mind, we modified the simulations to discard the approximately one-third most ambiguous configurations.

The purpose of the second simulation was to explore how the value of the spatial match threshold influenced the selection and alignment of particles. A moderate amount of noise, up to 3.5 Å in a random direction (for a total range of the radius of a Nanogold particle), was added to the rotated cluster coordinates before projection to represent the sum of noise in the position of the heavy atom cluster with respect to the particle and noise in imaging and locating the center of the cluster. For each of 300 randomly generated cluster configurations, 300 particles were rotated randomly and aligned using spatial match thresholds from 0 Å to 6 Å (Fig. 2). In addition, for each of 300 randomly generated cluster configurations, 300 particles were deformed by randomly displacing one cluster, selected at random, by 14 Å before projection. This deformation models a rotation of one domain of a 500-kDa protein (expected radius 52 Å) about the center of mass by 10°. Such a movement is fortuitously amplified by the length of the scFv, which will likely place the heavy atom cluster about another 28 Å away from the protein surface, so that the total radial arm is 80 Å. The resulting projections were matched against the original, undeformed cluster configurations by using the same range of spatial match thresholds.

The results showed that the spatial match threshold set a balance between the efficiency of particle alignment and the selective power of the method. This can be understood by considering a randomly rotated particle to which clusters are flexibly attached. The projected cluster positions in an image are the average cluster positions, as dictated by the rotation angles and the original cluster coordinates, plus a random displacement because of the various sources of noise. To orient the particle, the rotation angles that produce a best-fit projection pattern are found, but some spatial match error because of the noise will remain. If the spatial match threshold is set to a low value, only the least noisy particles are matched to rotation angles and used for averaging. If the spatial match threshold is increased, more and more noisy particles can be aligned, decreasing the total number of particles that have to be imaged and considered. The higher the spatial match

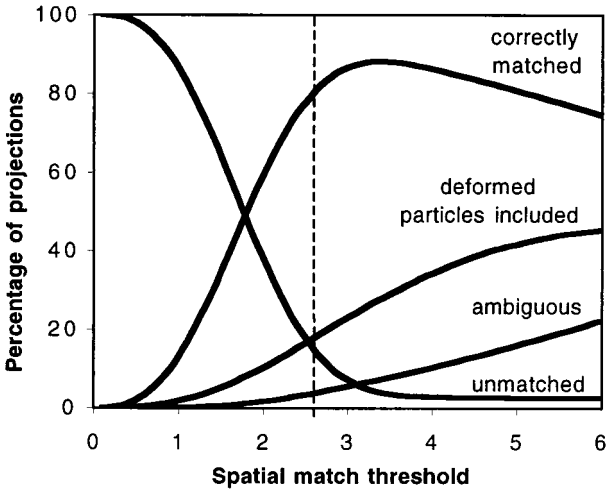

FIG. 2. Influence of spatial match threshold. Three hundred randomly rotated particle projections of each of 300 cluster configurations were simulated with ±3.5-Å random noise added and aligned using a range of spatial match thresholds. The percentages of correctly matched particles, unmatched particles, and ambiguous particles at each threshold are shown, while the final category (mistakenly matched particles), which makes up the remaining percentage, is not shown. In addition, the same number of particles, deformed to model a 10° domain shift, were also subjected to the alignment procedure, and the percentage included (eluding detection) is shown.

threshold, however, the more likely it is that projection patterns from other, closely related or widely different sets of rotation angles will also match the observed pattern, making the particle orientation ambiguous. Moreover, increasing the spatial match threshold makes it more likely that deformed particles will be included, and the selective power of the method is diminished. For 3.5-Å noise, a good choice for the spatial match threshold is 2.7 Å (indicated by the broken line in Fig. 2), where 83% of particles were aligned correctly, 12% were unmatched, 4% were ambiguous, 1% were mistakenly matched (not shown), and only 19% of deformed particles went undetected.

Alignment Errors. The third simulation explored how increasing noise in the cluster positions affected the angular alignment error. Five hundred random configurations of four clusters were rotated with 500 random sets of rotation angles each, and various levels of noise were added to the recorded projection positions before rotation angles were found. The median angular error between the actual angles used to rotate the particle and the angles found by the alignment procedure was calculated (Table 1, column 4). Optimal spatial match thresholds were chosen empirically. The results of this simulation showed that the median angular error for correct matches varied from 0° to 1.7° as noise increased from 0 Å to a full diameter of a Nanogold particle (±7 Å). The expected angular error for noise of ±7 Å, based on the inverse sine of the average cluster displacement because of noise (3.5 Å) divided by the average radial distance from the origin to the cluster (80 Å) as described above, is 2.5°. Thus the presence of four clusters, allowing best-fit angles to be found, significantly reduced the alignment errors. To relate the angular errors to the resolution attainable in a reconstruction, we note that for a 500-kDa protein of expected radius 52 Å, a 1.54-Å carbon-carbon bond at the surface subtends an angle of 1.7°. Thus even at high levels of noise, single-particle alignment with heavy atom clusters should allow particle orientation adequate for atomic resolution reconstructions.

Selection. The final simulation was designed to explore the usefulness of the proposed method in selecting a homogeneous population of single particles for averaging. Inhomogeneity

can arise from a number of sources, including stoichiometry, conformational state, mechanical deformation, and so forth. Binding of scFv-cluster conjugates to particles would clearly be useful in establishing stoichiometry, as epitopes could be chosen to identify components known to occur at low occupancy. To investigate effects of conformational shift or deformation, a simulation was performed as described above except that the coordinates of one cluster, selected at random, were displaced randomly by 61 Å before projection, which corresponds to a 45° movement of an 80-Å radial arm (Table 1, column 5). With a level of noise (±3 Å) near half the diameter of a Nanogold particle, more than 97% of the deformed particles were excluded (failed to match).

DISCUSSION

The proposed method preserves the advantages of cryoelectron microscopy and single-particle analysis, and it may overcome limitations on resolution. The advantages include the requirement for very little material, no need for crystalline or otherwise ordered arrays, the possibility of analyzing very large and even partially heterogeneous or disordered objects, and structure determination in the native state. Previous studies have been hampered by problems with selection and alignment of images. These problems were reduced by recording the images at high defocus values (2 μm or more), with consequent decay of the contrast transfer function, a likely factor in the ultimate limitation to about 20-Å resolution (30, 31). Although the development of more coherent electron beams may reduce the loss of high-resolution detail in highly defocused images (32, 33), imaging near focus will always be preferable because phase contrast is optimal at Scherzer focus (34) and because near focus the contrast transfer function undergoes fewer modulations requiring computational correction. The approach that we put forward here employs heavy atom clusters, which differ from biological material in an important way: they are revealed in the electron microscope by strong amplitude contrast as well as phase contrast. Heavy atom clusters are therefore visible at very low dose, and they are most clearly distinguished close to focus, where amplitude contrast dominates the image. For these reasons, heavy atom clusters have potential for particle selection and alignment under imaging conditions optimal for collection of high-resolution detail.

The three biological specimens so far solved to near atomic resolution by electron microscopy were all two-dimensional crystals, preserved in a partially dehydrated state, and imaged at defocus values less than 1 μm (2, 5, 6). Studies of helical crystals and of icosahedral viruses preserved in the frozen, hydrated state and imaged at higher defocus values have attained somewhat lower resolution, allowing visualization of secondary structure for tobacco mosaic virus (35), nicotinic acetylcholine receptor (36), bacterial flagellar filaments (37, 38), papillomavirus (39), and hepatitis B virus (40, 41). Despite the appeal of frozen specimens for generality and for retention of the native state, they suffer from lower contrast at high resolution, possibly because the low mechanical strength of ice allows greater particle movement (42). The use of heavy atom clusters may allow the selection of images free from this defect and others, such as astigmatism, on the basis of the shape and fine edge details of the clusters. Indeed, Nanogold has been suggested as a standard specimen to investigate the effects of specimen drift and charging (42). Heavy atom clusters may also identify images suffering from variation in magnification within a single micrograph (39) by the uniform spreading of projection patterns.

A further advantage of alignment and selection based on heavy atom clusters is speed, permitting more particles to be averaged, leading to higher-resolution 3-D reconstructions. The number of particles averaged [approximately 5 million for crystallographic analysis of bacteriorhodopsin (43) versus 2–6 thousand for single-particle analysis of ribosomes and viruses] is surely now a limiting factor in single-particle analysis. Current strategies for iterative alignments based on growing sets of common lines, often accompanied by multivariate statistical analysis to select homogeneous populations of particles (10), are computationally intensive. In contrast, the selection and alignment strategy used in our simulations accomplished both tasks at over 200 particles per second (on a 533-MHz, quad-issue DEC alpha running OSF), and required minimal memory. As specimen preparation, microscope operation, image acquisition, and processing become increasingly automated, the selection and alignment strategy we have proposed would not be rate limiting.

Binding scFvs to a particle as proposed here could also help in obtaining the full range of views required for 3-D reconstruction. Single-particle analysis currently suffers from a tendency of the particles to adopt only a small number of preferred orientations. Because four scFvs together have more than half the expected surface area of a 500-kDa protein (assuming spherical particles with uniform density), various combinations should significantly affect the surface properties and allow the presentation of multiple orientations. In addition, scFvs prepared with affinity tags will dominate the orientations of particles bound to a cognate surface, for example, scFvs bearing hexahistidine tags bound to a Ni-chelating surface.

Although the feasibility of the proposed method has not been tested experimentally, several studies have been performed involving Nanogold derivatives of single particles and cryoelectron microscopy (12–18). In this work, the feasibility of imaging Nanogold under low-dose conditions, close to focus, frozen in thin layers of vitreous ice was demonstrated, as noted above. In one case, a selection was performed in which particles with a single Nanogold in either a central or a peripheral location were averaged into independent sets (18). Colloidal gold unattached to any particle has also been used to align fixed, embedded thin sections for tomographic analysis (28). No observations have been reported that would raise fundamental concerns about our proposed approach of rigid attachment of multiple heavy atom clusters for selection and alignment of electron micrographs recorded close to focus under low-dose conditions.

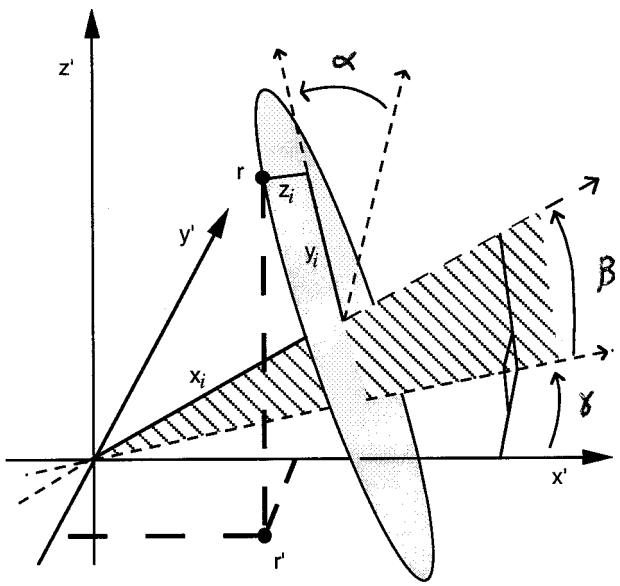

FIG. 3. Coordinate systems and rotation angles. The primed coordinate system x', y', z' represents the lab reference frame, and the position r' (x_i', y_i') is the projection of a cluster with coordinates r (x_i, y_i, and z_i) in the particle coordinate system after the particle has been rotated by the angles γ, then β, then α. Such a point not on the particle x-axis will travel along a circular pathway as α varies at constant β and γ. The projection of this circle onto the $x'y'$ plane is an ellipse.

APPENDIX

Two coordinate systems were established, one with respect to the particle and one with respect to the lab. To define the particle coordinate system, the origin was placed at the clusters' center of mass. Next the direction to the furthest cluster from the origin (designated no. 1) was chosen as the *x*-axis, and the *xy* plane was chosen to contain the second furthest cluster from the origin (designated no. 2) within quadrant 1 or 2. The coordinate system with respect to the lab was defined as the particle coordinate system before rotation. Rotations were accomplished through a positive rotation γ around the particle *z*-axis, then a negative rotation β around the particle *y*-axis, and finally a positive rotation α around the particle *x*-axis (Fig. 3).

After translating a set of projected cluster coordinates (primed) so that their center of mass was the origin, the following equation related them to the original cluster coordinates in the particle coordinate system (unprimed):

$$\begin{pmatrix} x'_1 & x'_2 & x'_3 & x'_4 \\ y'_1 & y'_2 & y'_3 & y'_4 \\ - & - & - & - \end{pmatrix} = \begin{bmatrix} \cos\gamma\cos\beta & -\cos\gamma\sin\beta\sin\alpha - \sin\gamma\cos\alpha & -\cos\gamma\sin\beta\cos\alpha + \sin\gamma\sin\alpha \\ \sin\gamma\cos\beta & -\sin\gamma\sin\beta\sin\alpha + \cos\gamma\cos\alpha & -\sin\gamma\sin\beta\cos\alpha - \cos\gamma\sin\alpha \\ \sin\beta & \cos\beta\sin\alpha & \cos\beta\cos\alpha \end{bmatrix} \begin{pmatrix} x_1 & x_2 & x_3 & x_4 \\ 0 & y_2 & y_3 & y_4 \\ 0 & 0 & z_3 & z_4 \end{pmatrix}.$$

The projected position of the first cluster alone yielded an initial estimate for β and γ:

$$\gamma = \tan^{-1}\left(\frac{y'_1}{x'_1}\right) \qquad \beta = \cos^{-1}\left(\frac{x'_1}{x_1\cos\gamma}\right).$$

At constant β and γ, the projection of any cluster not on the particle *x*-axis will trace out an ellipse in the $x'y'$ plane (lab coordinate system) as α varies. An initial estimate for α was therefore obtained by projecting the second cluster's position onto the major axis of its ellipse. To do this, its *y* coordinate in the lab system was rotated by γ about the z' axis (y now shown double primed), and then α was found with an inverse cosine function:

$$\begin{aligned} r &= \sqrt{(x'_2)^2 + (y'_2)^2} & \theta &= \tan^{-1}\left(\frac{y'_2}{x'_2}\right) \\ y''_2 &= r\sin(\theta - \gamma) & \alpha &= \cos^{-1}\left(\frac{y''_2}{y_2}\right) \end{aligned}.$$

These initial estimates of α, β, and γ were iteratively refined to minimize the sum of the squared errors in each of the eight equations present in the matrix expression above.

We thank Sarah Harris, Dan Millward, Dave Bushnell, Patrice Koehl, Max Vasquez, Jay Tso, and Naoya Tsurushita for helpful discussions. We thank Aaron Klug, Michael Levitt, James Hainfeld, Seth Darst, Ken Downing, and Arun Malhotra for comments on the manuscript. G.J.J. was supported by a Medical Scientist Training Program grant (GM07365) provided by the National Institute of General Medical Sciences at the National Institutes of Health. This research was supported by National Institutes of Health Grant AI21144 to R.D.K.

1. Klug, A. & Berger, J. E. (1964) *J. Mol. Biol.* **10,** 565–569.
2. Henderson, R., Baldwin, J. M., Ceska, T. A., Zemlin, F., Beckman, E. & Downing, K. H. (1990) *J. Mol. Biol.* **213,** 899–929.
3. Downing, K. H. (1991) *Science* **251,** 53–58.
4. Erickson, H. P. & Klug, A. (1971) *Philos. Trans. R. Soc. London B* **261,** 105–118.
5. Kühlbrandt, W., Wang, D. N. & Fujiyoshi, Y. (1994) *Nature (London)* **367,** 614–621.
6. Nogales, E., Wolf, S. G. & Downing, K. H. (1998) *Nature (London)* **391,** 199–202.
7. Crowther, R. A. & Klug, A. (1975) *Annu. Rev. Biochem.* **44,** 161–182.
8. Amos, L. A., Henderson, R. & Unwin, P. N. T. (1982) *Prog. Biophys. Mol. Biol.* **39,** 183–231.
9. Uzgiris, E. E. & Kornberg, R. D. (1983) *Nature (London)* **301,** 125–129.
10. Frank, J., Radermacher, M., Penczek, P., Zhu, J., Li, Y., Ladjadj, M. & Leith, A. (1996) *J. Struct. Biol.* **116,** 190–199.
11. Hainfeld, J. F. & Furuya, F. R. (1992) *J. Histochem. Cytochem.* **40,** 177–184.
12. Wenzel, T. & Baumeister, W. (1995) *Struct. Biol.* **2,** 199–204.
13. Braig, K., Simon, M., Furuya, F., Hainfeld, J. F. & Horwich, A. L. (1993) *Proc. Natl. Acad. Sci. USA* **90,** 3978–3982.
14. Spin, J. M. & Atkinson, D. (1995) *Biophys. J.* **68,** 2115–2123.
15. Wagenknecht, T., Brassucci, R., Berkowitz, J., Carbone, K., Furuya, F. & Hainfeld, J. (1992) *FASEB J.* **6,** A469 (abstr.).
16. Wagenknecht, T., Berkowitz, J., Grassucci, R., Timerman, A. P. & Fleischer, S. (1994) *Biophys. J.* **67,** 2286–2295.
17. Boisset, N., Grassucci, R., Penczek, P., Delain, E., Pochon, F., Frank, J. & Lamy, J. N. (1992) *J. Struct. Biol.* **109,** 39–45.
18. Wilkens, S. & Capaldi, R. (1992) *Arch. Biochem. Biophys.* **299,** 105–109.
19. Teo, B. K., Shi, X. & Zhang, H. (1992) *J. Am. Chem. Soc.* **114,** 2743–2745.
20. Teo, B. K., Zhang, H. & Shi, X. (1990) *J. Am. Chem. Soc.* **112,** 8552–8562.
21. Ladenstein, R., Bacher, A. & Huber, R. (1987) *J. Mol. Biol.* **195,** 751–753.
22. Fenske, D., Ohmer, J. & Hachgenei, J. (1985) *Angew. Chem. Int. Ed. Engl.* **24,** 993–995.
23. Ceriotti, A., Fait, A., Longoni, G. & Piro, G. (1986) *J. Am. Chem. Soc.* **108,** 8091–8092.
24. Mednikov, E., Eremenko, N. K., Slovokhotov, Y. L. & Struchkov, Y. T. (1987) *J. Chem. Soc. Chem. Commun.* **1342,** 218–219.
25. Milligan, R. A., Whittaker, M. & Safer, D. (1990) *Nature (London)* **348,** 217–221.
26. Lesk, A. M. & Chothia, C. (1988) *Nature (London)* **335,** 188–190.
27. Starink, J. P. P., Humbel, B. M. & Verkleij, A. J. (1995) *Biophys. J.* **68,** 2171–2180.
28. Skoglund, U., Andersson, K., Strandberg, B. & Daneholt, B. (1986) *Nature (London)* **319,** 560–564.
29. Glaeser, R. M., Tong, L. & Kim, S.-H. (1989) *Ultramicroscopy* **27,** 307–318.
30. Stark, H., Mueller, F., Orlova, E. V., Schatz, M., Dube, P., Erdemir, T., Zemlin, F., Brimacombe, R. & van Heel, M. (1995) *Structure* **3,** 815–821.
31. Frank, J., Zhu, J., Penczek, P., Li, Y., Srivastava, S., Verschoor, A., Radermacher, M., Grassucci, R., Lata, R. K. & Agrawal, R. (1995) *Nature (London)* **376,** 441–444.
32. Zhou, Z. H. & Chiu, W. (1993) *Ultramicroscopy* **49,** 407–416.
33. Zemlin, F. (1994) *Micron* **25,** 223–226.
34. Scherzer, O. (1948) *J. Appl. Phys.* **20,** 20–29.
35. Jeng, T.-W., Crowther, R. A., Atubbs, G. & Chiu, W. (1989) *J. Mol. Biol.* **205,** 251–257.
36. Unwin, N. (1993) *J. Mol. Biol.* **228,** 1101–1124.
37. Mimori, Y., Yamashita, I., Murata, K., Fujiyoshi, Y., Yonekura, K., Toyoshima, C. & Namba, K. (1995) *J. Mol. Biol.* **249,** 69–87.
38. Morgan, D. G., Owen, C., Melanson, L. A. & DeRosier, D. J. (1995) *J. Mol. Biol.* **249,** 88–110.
39. Trus, B. L., Roden, R. B. S., Greenstone, H. L., Vrhel, M., Schiller, J. T. & Booy, F. P. (1997) *Nat. Struct. Biol.* **4,** 413–420.
40. Bottcher, B., Wynne, S. A. & Crowther, R. A. (1997) *Nature (London)* **386,** 88–94.
41. Conway, J. F., Cheng, N., Zlotnick, A., Wingfield, P. T., Stahl, S. J. & Steven, A. C. (1997) *Nature (London)* **386,** 91–94.
42. Henderson, R. (1992) *Ultramicroscopy* **46,** 1–18.
43. Henderson, R. (1995) *Q. Rev. Biophys.* **28,** 171–193.